Available online at www.sciencedirect.com

SCIENCE DIRECT

Diamond & Related Materials 13 (2004) 1873–1881

DIAMOND AND RELATED MATERIALS

www.elsevier.com/locate/diamond

Molecular dynamics simulations for the growth of diamond-like carbon films from low kinetic energy species

Erik Neyts[a,*], A. Bogaerts[a], R. Gijbels[a], J. Benedikt[b], M.C.M. van de Sanden[b]

[a] Department of Chemistry, University of Antwerp, Universiteitsplein 1, Antwerp, Wilrijk B-2610, Belgium
[b] Department of Applied Physics, Eindhoven University of Technology, P.O. Box 513, Eindhoven 5600 MB, The Netherlands

Received 16 October 2003; received in revised form 16 April 2004; accepted 20 May 2004
Available online 28 July 2004

Abstract

In this study, molecular dynamics simulations using the Brenner potential for hydrocarbons have been used to simulate the formation of diamond-like carbon (DLC) films grown from low-energy hydrocarbon radicals (<2 eV). With these simulations, insight is gained in the processes occurring in this type of deposition. The initial surface is a previously deposited DLC surface; impinging particles include Ar^+ ions, with an energy of 2 eV, as well as several carbon radicals and molecules, and hydrogen atoms, with an energy of 1 eV. Two different radical flux compositions were examined: in the first condition, only C, C_2, and CH were used as growth species, as well as a large flux of H atoms. In the second condition, the same carbon radicals were considered, as well as the C_2H radical and C_2H_2, C_4H_2, and C_6H_2 molecules, but without the H atom flux. These fluxes are similar to different experimental conditions in an expanding thermal Ar/C_2H_2 plasma (expanding thermal plasma, or ETP), using different influxes of acetylene. Several properties of the resulting films will be presented, focusing mainly on the carbon coordination and the bonding network. The simulations suggest that lowering the acetylene influx results in films having a more extensive bonding network, but with more H incorporated. This leads to more polymeric films having a less diamond-like character, as is expected also from experiments. The aim of this work is twofold. The first objective is to compare the structural composition of the simulated films to the structure of the experimentally deposited films by applying similar conditions. Second, the simulations can give us valuable information about the key mechanisms in the deposition process.
© 2004 Elsevier B.V. All rights reserved.

Keywords: MD simulation; Diamond-like carbon

1. Introduction

Diamond-like carbon (DLC) films are important technological materials with widespread applications, such as antifuses [1], biocompatible coatings [2], or coatings of magnetic hard disks [3]. Many different ways to produce DLC are being used, depending on the desired film properties. Amongst others, ion beam deposition [4], sputtering [5], plasma-enhanced chemical vapor deposition (PECVD) [6,7], and pulsed laser deposition [8] are most frequently used. A comprehensive review of the preparation, properties, and characterisation of DLC can be found in Ref. [9].

Since the properties of the deposited film depend on the atomic composition and microscopic structure of the film, continuous efforts are being made to characterize these materials. However, no experimental method exists for the determination of this microscopic structure in three dimensions. Therefore, simulation methods are an invaluable tool used to investigate the mechanisms behind the deposition process and resulting film characteristics. The most widely used methods for simulating the deposition process are molecular dynamics (MD) simulations, since they allow to follow the evolution of a system of particles on the atomic level (e.g., see Refs. [10,11]). In these simulations, the most widely used potentials are those suggested by Brenner [12] and Tersoff [13], being semiempirical many-body potentials. A more fundamental approach involves the use of tight-binding potentials (e.g., see Ref. [14]).

It is generally accepted that the formation of sp^3-rich DLC films is associated with the subsurface implantation of C-containing species (“subplantation”) [9]. This, however, requires a flux of high-energy particles, leading to physical

* Corresponding author. Tel.: +32-3-820-23-82; fax: +32-3-820-23-76.
E-mail address: erik.neyts@ua.ac.be (E. Neyts).

0925-9635/$ - see front matter © 2004 Elsevier B.V. All rights reserved.
doi:10.1016/j.diamond.2004.05.011

growth of the film. In the present work, however, we focus on the growth of DLC films from low-energy hydrocarbons (<2 eV), such that subplantation cannot occur. Under these circumstances, films can only grow by chemisorption and reconnection of the network. These studies are relevant for remote-type plasmas such as, for example, the expanding thermal plasma (ETP) [18].

In Section 2, a description of the simulation model will be given. Next, the results will be presented, including the general microscopic structure of the films, the coordination of the carbon atoms, the effects of the different fluxes on the growth mechanism, and their effects on the resulting film properties. Finally, a summary and a conclusion will be given.

2. Description of the model

The simulation model presented in this paper was initially developed by Serikov et al. [15]. In an MD model, all atoms in the system are traced by Newtonian mechanics. Particles move under the influence of forces, derived from an interatomic potential. In this work, the Brenner potential [12] is used. The atom's spatial trajectory is integrated explicitly by using the velocity Verlet scheme [16]. The initial surface on which the growth of the a-C:H film is initiated was a previously simulated DLC film containing 712 atoms. The lower 128 atoms were kept static (corresponding to about two atomic layers) to anchor the simulation cell and to simulate a thick substrate. This initial substrate was produced by growing a film on a nonpassivated, nonreconstructed diamond {111} surface, at a temperature of 523 K. The method and growth species used to produce this initial substrate are the same as for the deposition of the DLC film under condition 1 (see below).

Periodic boundary conditions were enforced in the $\pm x$- and $\pm y$-directions. The substrate temperature was kept constant at 523 K, using the Berendsen heat bath algorithm [17]. An invariable timestep of 0.5 fs was chosen. The deposition process was simulated by exposing the substrate continuously to hydrocarbon species and Ar^+ ions. The species bombarding the substrate, as well as their energies and fluxes, are adopted from a specific experimental deposition of DLC films from an expanding thermal C_2H_2/Ar plasma by Benedikt et al. [18] and are given in Table 1. All impacts are normal to the surface, with a predefined energy of 1 eV per molecule for hydrocarbons, and 2 eV for the Ar^+ ions. The incident particle was initially placed at a distance above the substrate beyond the cutoff of the potential. The position in the x- and y-directions was chosen randomly. Each trajectory is run for 1500 timesteps, equal to 0.75 ps per impact. The number of impacts for every species is given below in Section 3.1.

Chemically speaking, particles can chemisorb or become reflected at the surface. Upon impact and subsequent chemisorption, bombarding molecules can either stick to the surface as a whole, or they can fragment, leaving one, several, or all fragments bound to the surface. In principle, particles can also physisorb at the surface, with subsequent diffusion over the surface. However, neither physisorption nor surface diffusion is included in the model at present. Implantation or subplantation events are not possible, considering the low energy of the impinging particles. Hence, these simulations are relevant for desposition processes involving no ion bombardment of the substrate.

Table 1
Species, fluxes, and energies of particles arriving at the substrate for both conditions, adopted from the experiments

Condition	Species	Flux ($\times 10^{21}$ s^{-1} m^{-2})	Energy (eV)
1	C_2H_2	0.0[a]	–
	Ar^+	2.300	2
	H	5.302	1
	C_2	1.330	
	CH	0.796	
	C	0.796	
2	C_2H_2	2.650	1
	C_2H	2.210	
	C_4H_2	1.330	
	C_6H_2	0.442	
	C_2	0.221	
	CH	0.133	
	C	0.133	

[a] Totally consumed in the plasma chemistry.

Reflected atoms, fragments, and molecules not bound to the surface are removed at the end of each trajectory. Films of about 2.5 nm were simulated. After deposition, the film is allowed to relax for 20 ps at a constant temperature of 523 K. Output data are gathered, averaging over the last 10 atomic configurations determined at intervals of 50 fs, thus corresponding to the last 0.5 ps of relaxation.

Results obtained in this way include the atomic H concentration in the film, carbon coordination, density of the film, and information about the structural properties. Also, radial distribution functions (RDFs) are calculated, and information is obtained concerning the formation of rings in the deposited film. In addition to this structural information, the results also include information about the role of the different growth species and the mechanisms governing the deposition process.

3. Results and discussion

3.1. Input data and the experimental data set

Simulations have been carried out for two different conditions. Experimentally, these conditions are similar to a different flux of C_2H_2 through the injection ring in the ETP. For condition 1, a low acetylene influx was assumed; for condition 2, the influx was assumed to be high. In both conditions, argon is present in the discharge, but only in condition 1 were Ar^+ ions detected at the substrate. As mentioned above, these simulations are relevant for depo-

sition sources such as the ETP source. This is a remote plasma, where the argon thermal plasma at subatmospheric pressure is first created in a cascaded arc with an argon flow. At a constant arc current, a constant flow of Ar^+ ions and electrons into the reactor is maintained. The argon thermal plasma expands into the low-pressure vessel. In this type of plasma, the electron temperature is below 0.3 eV, resulting in a low substrate self-bias (<2 eV) and hence negligible ion bombardment on the sample during the deposition. Further details on the operation of the ETP can be found in Refs. [18,19] and references therein.

Electron energy loss spectroscopy (EELS) was used to investigate the bonding of the experimentally deposited films [20].

The species included here were chosen on the basis of cavity ring down spectroscopy (CRDS) measurements [18]. The flux values for the H atoms, however, were estimated to correspond to the experimental H concentration in the film, since no experimental data on the H flux were available. The H flux for the second condition was assumed to be zero, implying that all the H atoms incorporated in the second film are due to the bombarding hydrocarbons only.

The species included in the model, along with their fluxes to the substrate, are given in Table 1 for both conditions. The absence of acetylene in condition 1 is due to the complete consumption of the acetylene in the plasma chemistry. It should be noted that the real fluxes have no real meaning here, since every trajectory for every particle was calculated for 1 ps. Therefore, only the relative fluxes are important, indicating the ratios of the impinging particles. Finally, it should also be mentioned that there is considerable uncertainty concerning the particle fluxes as determined experimentally.

For the first film, which was deposited under condition 1, 2304 atom and molecule impacts were performed on the surface, of which 510 Ar^+ ions, 1158 H and 188 C atoms, and 278 C_2 and 170 CH radicals are present. The net result is the addition of 1019 atoms to the film, of which 466 H atoms and 553 C atoms are present. For the second film, deposited under condition 2, there were 1597 atom and molecule impacts on the surface, of which 583 C_2H_2, 312 C_4H_2, 104 C_6H_2, 487 C_2H, 46 C_2, 33 C, and 32 CH radicals were present . In total, 954 atoms were added to the surface, of which 283 H atoms and 671 C atoms were present.

3.2. General microscopic structure of the deposited films

In Fig. 1a and b, the simulated microscopic picture of both deposited films is shown. The film deposited under condition 1 (called here in brief "first film") is 24 Å thick, and the second film is 28 Å thick. These pictures already show a few general characteristics of both films: the first film shows fewer voids and more four-coordinated carbons than the second film. Also, the second film is somewhat thicker than the first film but has a lower density. It is also clear from the pictures that the H concentration in the first film is higher than in the second film. Also, the microcrystalline structures differ in both films. These characteristics will be explained in the following sections.

Also the occurrence of rings in both networks has been determined, as shown in Table 2. No rings with more than six members were found and only one aromatic ring was found: a six-membered ring in film 2. All other rings consist of a mixture of three-coordinated and four-coordinated carbons. However, the simulated films are too small, and they contain not enough atoms to draw definite conclusions from these data.

3.3. Coordination in the films and mechanisms of film growth

In the bulk, the average coordination number for the first film is calculated to be 3.4; for the second film, it is 2.7. The model as it is used for this work does not allow to calculate the hybridisation of the atoms in the deposited films. Therefore, one of the most important characterising properties of DLC on the microscopic level (i.e., the sp^3 fraction) cannot be calculated. Instead, the fraction of fourfold coordinated carbon atoms is calculated. In Fig. 2, this fraction, for the two conditions, is shown as a function of depth in the film.

It can be seen in the figure that the fourfold coordination heavily fluctuates with depth in the film, and becomes zero near the surface (right hand side of the figure). In the first film, the top 3 Å contains no fourfold coordinated atoms; in the second film, there are no fourfold coordinated atoms in the top 5 Å.

The fact that no fourfold coordination is present in the top few angstroms of both films is a consequence of the growth mechanism: since no high-energy particles are present, there can be no subplantation. Therefore, the films grow by chemisorption of incoming radicals on the surface. Hence, almost every incoming atom will initially be either onefold, twofold, or threefold coordinated. Therefore, for an atom to become fourfold coordinated, it must be covered by new incoming atoms such that it becomes embedded in the bulk.

From Fig. 2, it is clear that the fourfold coordination number in the bulk is higher in film 1 than in film 2. This can also be seen in Fig. 1a and b. For the first film, the fraction of four-coordinated carbons in the bulk is, on average, 0.50; for the second film, this fraction in the bulk is, on average, 0.16. It is worth mentioning that in order to calculate the fourfold coordination in the bulk, the upper atomic film included must be covered by at least one more complete monolayer. For condition 1, this upper monolayer is situated at 16.0 Å; for the second condition, it is located at 19.0 Å.

Since the hybridisation of the atoms cannot be determined in this model, a direct comparison with experi-

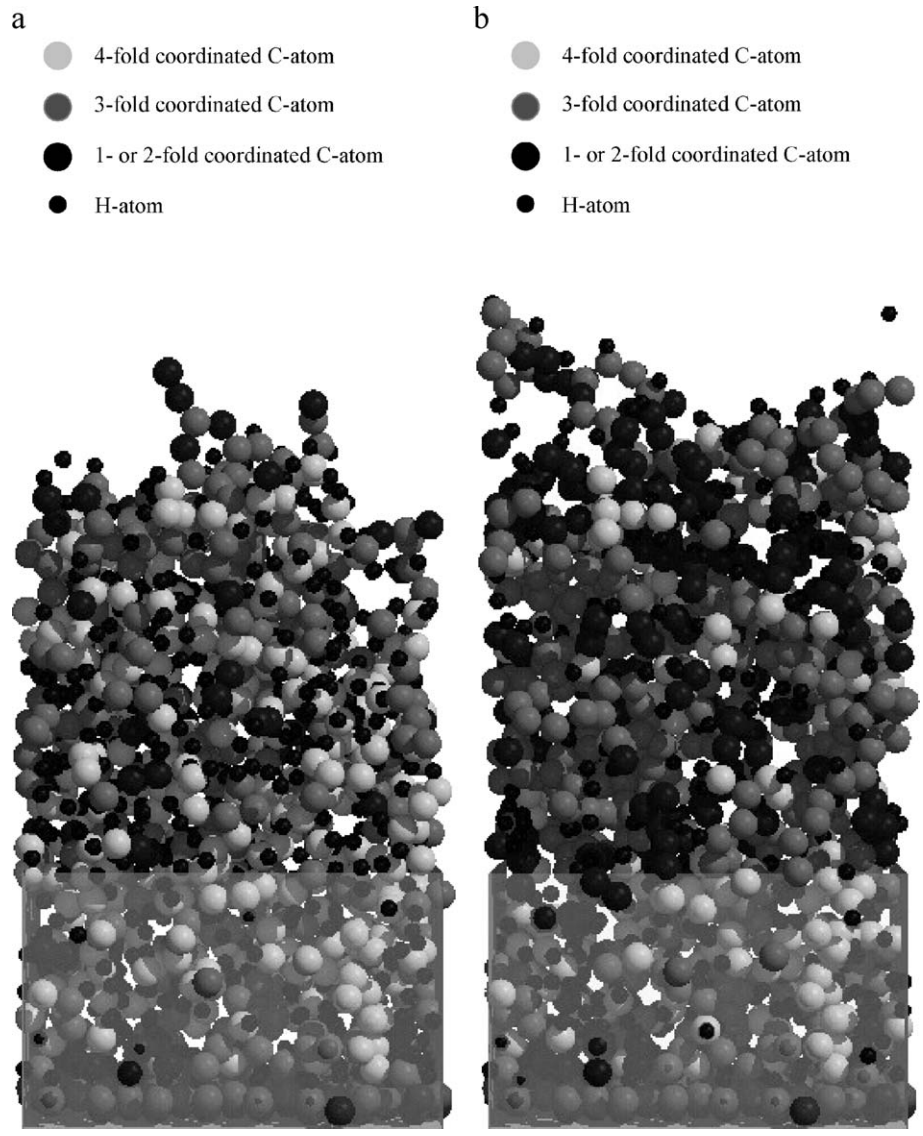

Fig. 1. Side view of the simulated films for condition 1 (a) and condition 2 (b). It can be seen that the film of condition 1 shows fewer voids in its structure, and contains a much higher fraction of fourfold coordinated carbon atoms, as compared to the film of condition 2.

ments is not possible. However, when we identify the fraction of fourfold coordinated carbon atoms with sp^3 hybridisation, an indirect comparison can be made. Experimentally, EELS measurements of the deposited films show an sp^3 fraction of 0.67 for the first film [20], which indicates a reasonable agreement with our simulated result of 0.50 for the fourfold coordinated fraction. The EELS data show a value of 0.53 for the sp^3 fraction in the second film [20], which is not in good agreement with our result of 0.16.

Table 2
Calculated occurrence of rings for both conditions

	Three-ring	Four-ring	Five-ring	Six-ring	> Six-ring
Film 1	2	1	3	1	0
Film 2	2	0	1	3	0

Two factors should be considered in interpreting this result. First, the uncertainties concerning the particle fluxes should be taken into account when comparing the simulation results and the experimental measurements, as well as the uncertainty regarding the EELS measurements [20]. These uncertainties are the same for both layers. Second, comparing the calculated fourfold coordinated fraction of the second film to the experimentally determined sp^3 fraction, it is clear that these values do not correspond, probably due to the fact that both the C_3H and the C_3H_2 radicals have not been included in the model. Indeed, recent preliminary measurements have revealed that these species are also formed in the plasma and could play a role in film growth under condition 2. Their effect on the resulting DLC film will be investigated in our future work.

The higher average coordination number and, more specifically, the higher fourfold coordination number pre-

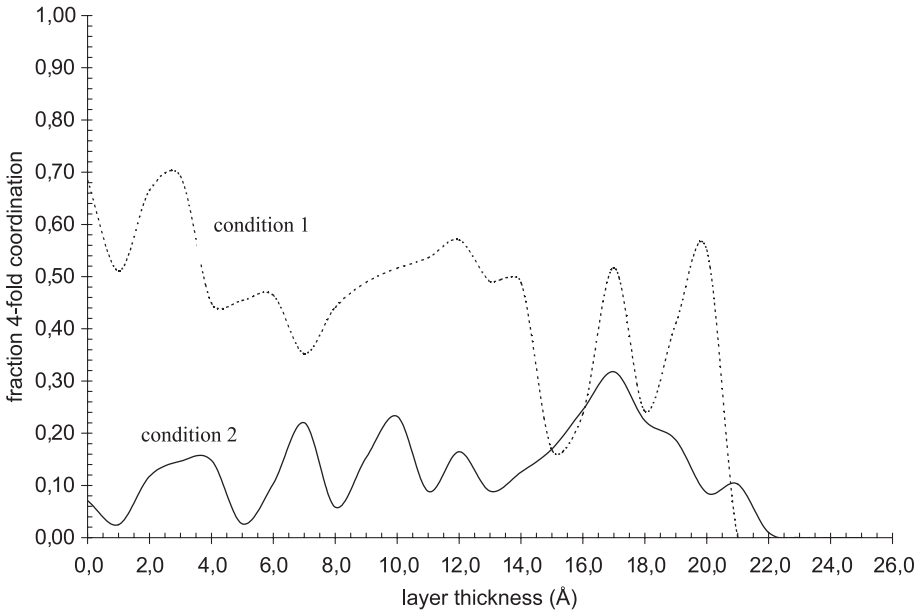

Fig. 2. Calculated fraction of fourfold coordinated carbon atoms for condition 1 (dashed line) and condition 2 (solid line) as a function of position in the film. The initial substrate on which the film was grown starts at 0.0 Å and extends to the left (not shown).

dicted by our model for the first film compared to the second film are results of the different growth species in both conditions. In Fig. 3, the sticking and etch efficiency of the different species are shown for both conditions. Only the species with a high sticking efficiency are shown. For condition 1, it is clear from the figure that not the H atoms, but the C_2 radical, is the most efficient etching species. In only 2.7% of the H impacts (corresponding to only 30 etch events) was material etched from the surface. The main etch product was H_2 (in 80.0% of the etch events). Also C_2H_2 and C_2H were etched, but to a minor extent. The C_2 radical, however, etches material away in 28.1% of its impacts, corresponding to 78 etch events. In 77 of these events, C_2H was the etch product, thus creating dangling bonds at the surface by removing hydrogen. In only one event was C_2H_2 the etch product. The same conclusion regarding the etch efficiency of C_2 can be made for condition 2: in all etch events, the etch product was C_2H. Although also under condition 2 the etch efficiency itself is rather high for C_2 (30.4%), the effect is small due to the very low relative flux of C_2: only 2.9% of the impacts under condition 2 is a C_2 radical. In total, only 14 H atoms were removed from the surface due to C_2 etching.

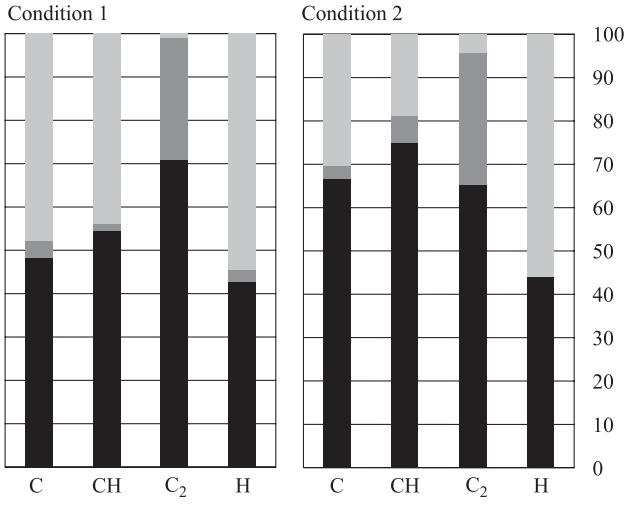

Fig. 3. Calculated sticking and desorption efficiencies of the main growth species under condition 1 (left panel) and condition 2 (right panel). The black areas indicate the sticking efficiencies, the dark grey areas indicate the etching efficiencies, and the light grey areas indicate the fraction of events where sticking nor etching occurred. Only the species with a high sticking efficiency are shown.

The contribution of the different species to the growth of the layer is shown in Fig. 4. For condition 1, the main growth species is found to be C_2, responsible for over 68% of the carbon atoms in the final film. This is a direct result of: (i) its high relative flux (43.6% of all C-containing species under condition 1 is C_2); (ii) the fact that it brings two carbon atoms to the surface per impact (60.7% of all carbon atoms arriving at the surface); and (iii) its high sticking efficiency (70.9%). The role of the H atoms is primarily to passivate dangling bonds: under these conditions, the H is not an efficient etching species, but simply binds to the surface in 42.8% of its impacts. Due to its high relative flux, it is the main source of hydrogen in the film under condition 1 (84.5%).

The most important growth species under condition 2 is C_2H: 63.4% of the C atoms and 70.5% of the H atoms in film 2 are incorporated through C_2H impacts. Only 6.8% of the carbon atoms in this film comes from growth species that do not have a double bond (i.e., C and CH). The most important growth species (i.e., C_2) under

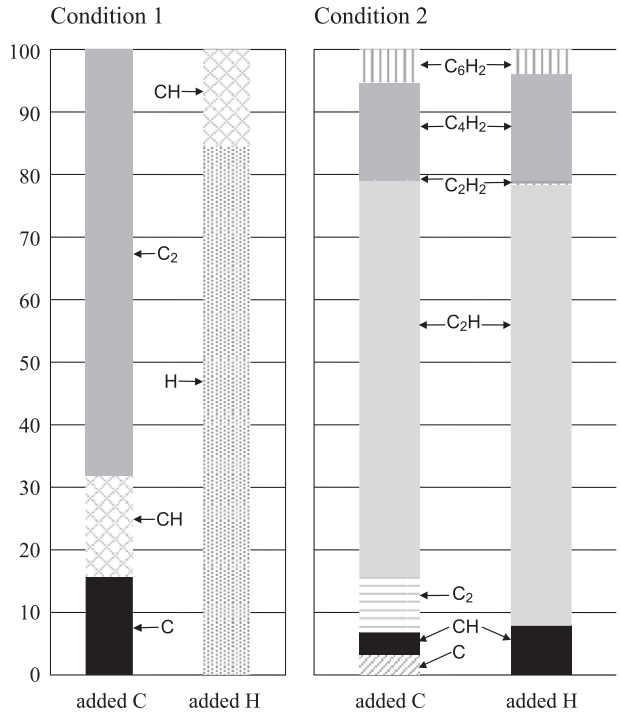

Fig. 4. Calculated contribution of the different species to the growth of the film, in terms of the fraction of carbon atoms and hydrogen atoms added to the film by each species, under condition 1 (left panel) and condition 2 (right panel).

condition 1 and C_2H under condition 2 both contain a triple bond. However, an impinging particle will more easily become fourfold coordinated when it has no double or triple bonds, since these species require that the double and triple bonds become saturated by incoming H atoms or incoming radicals in order to become fourfold coordinated. In condition 1, all growth species are very reactive, and more than 30% of the carbon added to the film comes from particles (C and CH) not having a double or triple bond. In condition 2, on the other hand, fourfold coordination is more difficult to obtain, since in this case, the most important growth species is C_2H. This radical has two resonance structures, with a double and a triple bond, respectively, resulting in a carbon–carbon bond order of 2.5. This carbon–carbon bond has to be saturated before fourfold coordination can occur. The same is true for C_4H_2 and C_6H_2: both are stable molecules containing triple bonds. Although both have a rather low sticking efficiency (8.3% for C_4H_2 and 5.8% for C_6H_2), they are responsible for 20.7% of the added carbon to the film. Also, there is no H flux present for this condition to saturate this unsaturated bond and to passivate dangling bonds at the growing surface. Both factors contribute to the dramatic lowering of the fourfold coordination compared to the first condition, as predicted with our model.

Also, while the twofold coordination in the first film is relatively low (0.09), it is very high in the second film (0.29). This is also a consequence of the nature of the growth species, which are highly unsaturated, as well as the lack of an atomic H flux. The higher fraction of fourfold coordination is also reflected in the RDF, which we will discuss in the next section.

3.4. The RDF

Equally important to determine the microstructure of the simulated films is to calculate the RDF and, more specifically, the 4–4 RDF, indicative for the fraction of fourfold coordinated C atoms bound to other fourfold coordinated C atoms. This fraction is important, since it constitutes the bonding network, giving the structure its mechanical hardness and rigidity.

The RDF measures the probability of finding an atom at a distance r from any other atom, relative to the same probability in an ideal gas at the same overall number density. Therefore, it constitutes a normalised distribution of interatomic distances. In a crystalline material like diamond, the atoms are situated at well-defined positions, and the RDF will therefore show well-defined peaks and valleys over a long scale length, implying long-range order. In an amorphous material, however, the atoms are not localised at well-defined positions; therefore, no peaks will appear in the RDF except at first neighbour distances.

In Fig. 5, the 4–4 RDF is shown for both DLC films, indicating the number of pairs of atoms both having four neighbours. It can be seen that there is no long-range order, as there are no peaks beyond ~ 2.65 Å, as is expected for these DLC films. There is, however, a medium-range order,

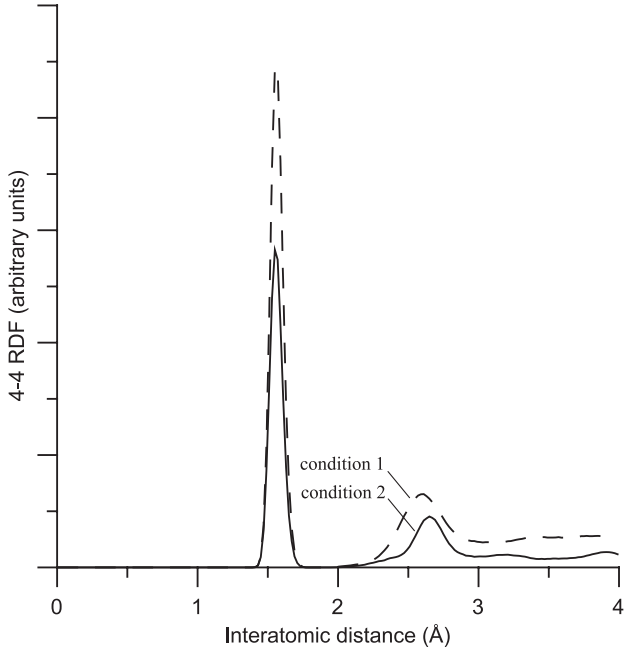

Fig. 5. Calculated 4–4 RDF for film 1 (dashed line) and film 2 (solid line).

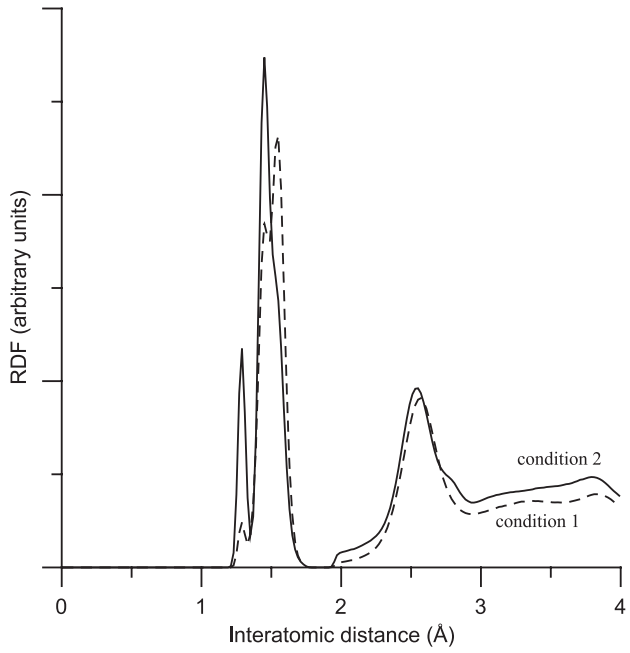

Fig. 6. Calculated total carbon–carbon RDF for film 1 (dashed line) and film 2 (solid line). The H atoms are not included in this RDF.

as indicated by the second peak at about 2.65 Å. Since the peak at 1.55 Å for film 1 is much larger than it is for film 2, the 4–4 RDF shows that there is much more 4–4 coordination in the first film. This indicates a more rigid structure. Also the second nearest neighbours are more strongly coordinated in the first film than in the second film, shown by the larger peak at 2.65 Å for film 1.

In Fig. 6, the total carbon–carbon RDF is shown for both films. The first peak, at about 1.3 Å, shows up due to twofold coordinated carbon atoms, bound to either other twofold coordinated carbon atoms, or threefold or fourfold coordinated carbon atoms. It can be seen that the second film contains a much larger fraction of twofold coordinated carbons.

The second peak, at about 1.5 Å, is split in two in the first film. The left peak arises from 3–3 coordinated carbon atoms, while the right peak is a combination of 3–4 and 4–4 coordinated carbon atoms. The importance of this overlap of the 3–3 and 4–4 peaks is diminished in the second film to a barely visible shoulder at the right of the main peak at 1.5 Å. This indicates that the fraction of 3–4 and 4–4 coordinated carbon atoms is greatly reduced in the second film as compared to the first film, while the 3–3 fraction is increased. Again, this reflects the lower fourfold coordination in the second film. The RDF therefore indicates that the first film has a more extensive bonding network than the second film. However, due to the much higher H content in the first film (resulting in many CH_2 and CH_3 structure fragments, see below), this does not lead to a more diamond-like character of the film, but rather to a more polymeric structure.

3.5. Hydrogen content of the films

The average hydrogen content of the films is calculated to be 0.46 for the first film and 0.30 for the second film. Experimentally, values of >0.42 and 0.35, respectively, were obtained [20]. The H fraction in both films, as a function of the film thickness, is shown in Fig. 7. It can be seen that the H content remains fairly constant throughout the film, except at the surface. The fraction of the different CH_x fragments in the films is shown in

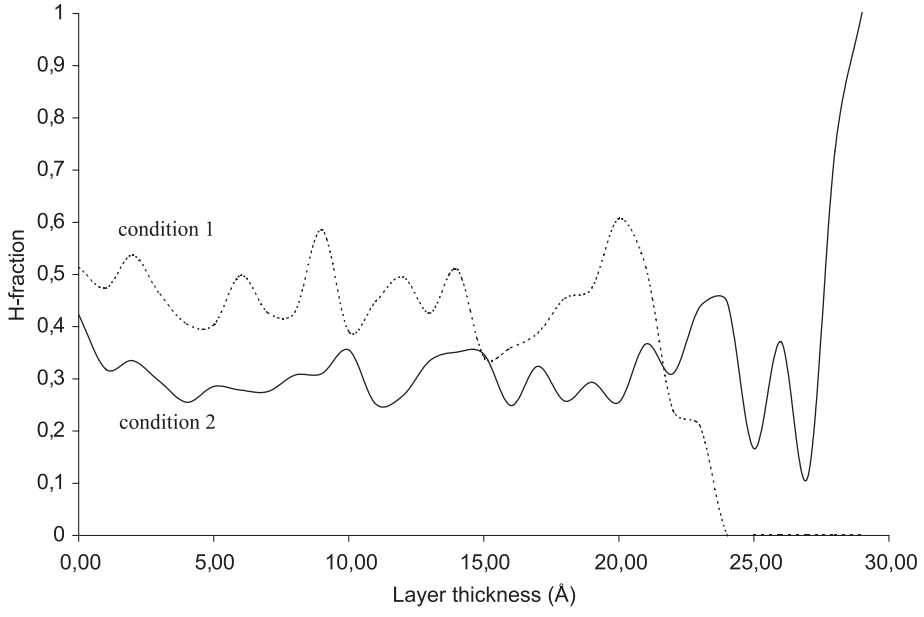

Fig. 7. Calculated H fractions for film 1 (dashed line) and film 2 (solid line), as a function of position in the film. The initial substrate starts at 0.0 Å and extends to the left (not shown).

Table 3
Calculated CH_x fractions in both films

	Condition 1	Condition 2
CH_0	0.353	0.515
CH_1	0.428	0.464
CH_2	0.196	0.021
CH_3	0.023	0

Table 3. Again there is a significant difference between the two films. The reason for this difference is the absence of an atomic H flux for the second condition, such that all the hydrogens present in the second film come from the growth species. The H fraction of 0.30 corresponds to C_2H and C_4H_2 as the main growth species. Since these growth species do not have carbon atoms with two or three hydrogen atoms, CH_2 and CH_3 fragments in the film can only be formed by breaking a C−H bond, followed by the migration of the H atom to a C atom that is already bound to a H atom. This explains the very low CH_2 and CH_3 fractions in the second film. In the first film, however, the incoming atomic H atoms can easily react with C atoms and CH radicals, which are not yet fully saturated.

3.6. Density of the films

In contrast to the large difference in coordination and hydrogen content, the density in both films is practically the same. The density in the bulk of the films is calculated to be 1.73 g/cm^3 for the first film and 1.75 g/cm^3 for the second film. This is a result of the higher fourfold coordination in the first film (increasing the density) combined with a higher hydrogen content (decreasing the density), relative to the second film.

The evolution of film density for both films as a function of film thickness is shown in Fig. 8. It can be seen that the density in both cases fluctuates, showing peaks every ~ 3 Å in film 1 and every ~ 2.5 Å in film 2. The peaks in the density evolution in both films appear at positions with a valley in the H content evolution, showing the inverse relation between hydrogen content and density. This effect is then balanced by the coordination number to result in similar densities in both films.

4. Summary and conclusion

The deposition of DLC films for two different conditions was investigated with MD simulations, using the Brenner potential. As an example, the fluxes used in the simulations were taken from ETP experiments under two different operating conditions (i.e., different influxes of acetylene through the injection ring of the ETP), resulting in different reactive species reaching the substrate. For the first condition, corresponding to a low influx of acetylene, a film was formed with a rather high fraction of fourfold coordinated carbon atoms (0.50), high hydrogen concentration in the film (0.46), and a rather low density of 1.73 g/cm^3, typical for this type of DLC. For the second condition, corresponding to a higher influx of acetylene, our simulations predict the formation of a film containing only a small fraction of fourfold coordinated carbon atoms (0.16), a lower H content (0.30), and a similar density (1.75 g/cm^3). The results for the first film correspond fairly well

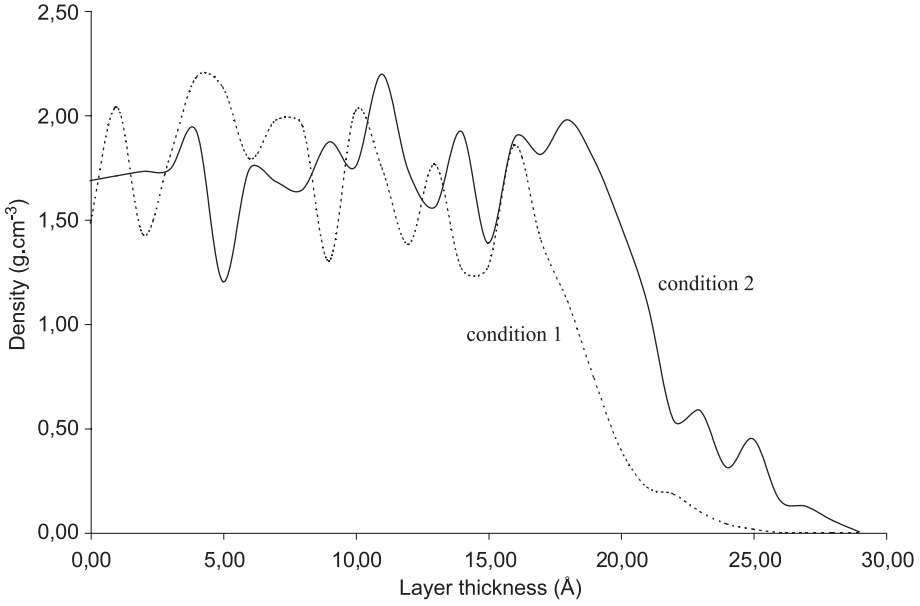

Fig. 8. Calculated density for film 1 (dashed line) and film 2 (solid line), as a function of position in the film. The initial substrate starts at 0.0 Å and extends to the left (not shown).

to the experimental data; the results for the second film, however, do not correspond so well to the experimental results. The reason is probably that the C_3H and C_3H_2 radicals, which are expected to be formed in the plasma under condition 2 as revealed by recent preliminary experiments, were not yet taken into account in the present model.

The results can be explained in terms of the growth mechanism, as well as the growth species and their fluxes towards the substrate. It is shown that under condition 1, the C_2 radical is both the most efficient and most important growth and etch species, while the H atoms are only passivating dangling bonds. More than 30% of the carbon added to the film comes from particles that have no double or triple bonds (C and CH). While the C_2 radical remains the most efficient etch species under condition 2, the C_2H radical becomes the most important growth species. Less than 7% of the carbon atoms in the film originates from C and CH. The RDF indicates that both films have different microstructures: the first film has more extensive coordination than the second film. However, it also contains much more hydrogen, which results in a more polymer-like structure, in agreement with experiments. These simulations suggest that experimental conditions, changing only one parameter in the depositing plasma (i.e., the acetylene influx), can have a significant influence on the resulting film characteristics due to the different species and particle fluxes to the substrate. These simulations also suggest that changing only the growth species, without changing the governing growth mechanism (chemisorption), leads to different films, irrespective of the source used to generate these growth species.

Acknowledgements

E. Neyts is indebted to the Institute for the Promotion of Innovation by Science and Technology in Flanders (IWT-Flanders) for financial support. A. Bogaerts is indebted to the Flemish Fund for Scientific Research (FWO-Flanders) for financial support. J. Benedikt is indebted to the Foundation of Fundamental Research on Matter (project 99TF24) for financial support. The authors would like to thank C. Abrams, who developed the original MD code, for the many interesting discussions.

References

[1] D.R. McKenzie, W.T. Li, E.G. Gerstner, Diamond Relat. Mater. 10 (2001) 230.
[2] V.-M. Tiainen, Diamond Relat. Mater. 10 (2001) 153.
[3] J. Robertson, Tribol. Int. 36 (2003) 405.
[4] F. Rossi, B. André, A. van Veen, E.E. Mijnarends, H. Schut, M.P. Delplancke, W. Gissler, J. Haupt, G. Lucazeau, L. Abello, J. Appl. Phys. 75 (1994) 3121.
[5] S. Logothetidis, M. Gioti, P. Patsalas, C. Charidtidis, Carbon 37 (1999) 765.
[6] P. Djemia, F. Tétard, F. Ganot, C. Met, M.I. DeBarros, L. Vandenbulcke, Surf. Coat. Technol. 151–152 (2002) 170.
[7] N.M.J. Conway, A.C. Ferrari, A.J. Flewitt, J. Robertson, W.I. Milne, A. Tagliaferro, W. Beyer, Diamond Relat. Mater. 9 (2000) 765.
[8] D.L. Pappas, K.L. Saenger, J. Bruley, W. Krakow, J.J. Cuomo, T. Gu, R.W. Collins, J. Appl. Phys. 71 (1992) 5675.
[9] J. Robertson, Mater. Sci. Eng. R37 (2002) 129.
[10] B.J. Garrison, P.B.S. Kodali, D. Srivastava, Chem. Rev. 96 (1996) 1327.
[11] Z. Huang, Z.Y. Pan, Y.X. Wang, A.J. Du, Surf. Coat. Technol. 158–159 (2002) 94.
[12] D.W. Brenner, Phys. Rev. B 42 (1990) 9458.
[13] J. Tersoff, Phys. Rev. B 38 (1988) 9902.
[14] K. Kohary, S. Kugler, Phys. Rev. B 63 (2001) 193404.
[15] V.V. Serikov, S. Kawamoto, C.F. Abrams, D.B. Graves, APS Proceedings of the "22nd Symposium on Rarefied Gas Dynamics," Sydney, 2000.
[16] W.C. Swope, H.C. Anderson, P.H. Berens, K.R. Wilson, J. Chem. Phys. 76 (1982) 637.
[17] H.J.C. Berendsen, J.P.M. Postma, W.F. van Gunsteren, A. DiNola, J.R. Haak, J. Chem. Phys. 81 (1984) 3684.
[18] J. Benedikt, K.G.Y. Letourneur, M. Wisse, D.C. Schram, M.C.M. van de Sanden, Diamond Relat. Mater. 11 (2002) 989.
[19] J.W.A.M. Gielen, P.R.M. Kleuskens, M.C.M. van de Sanden, L.J. van Ijzendoorn, D.C. Schram, E.H.A. Dekempeneer, J. Meneve, J. Appl. Phys. 80 (1996) 5986.
[20] A.-L. Hamon, J. Verbeeck, D. Schryvers, J. Benedikt, M.C.M. van de Sanden, J. Mater. Chem. 14 (2004) 2030.